

Influence of Building Block Symmetry on the Band Structure of Stacked 2D Polyimide Covalent Organic Frameworks

Published as part of ACS Omega virtual special issue "Jaszowiec 2023".

Mateusz Wlazło,* Keiichiro Maegawa, and Atsushi Nagai*



Cite This: ACS Omega 2023, 8, 47913–47918



Read Online

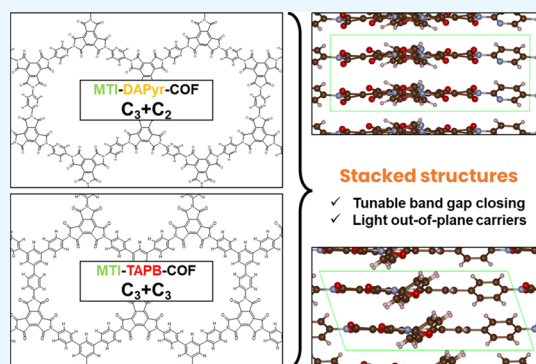
ACCESS |

Metrics & More

Article Recommendations

Supporting Information

ABSTRACT: Covalent organic frameworks (COFs) are a class of crystalline porous materials distinctively built solely from organic elements, carbon, oxygen, hydrogen, and often nitrogen or boron. They form light, mechanically rigid, and chemically stable networks that have many advantages, but their low solubility and poor processability create issues with developing large-scale films or membranes. Two-dimensional (2D) COFs possess periodic porous crystallinity, functionality, modularity, and layered one-dimensional (1D) transport channels. All of these traits, along with the semiconducting properties of selected COFs, make them interesting candidates for integration in optoelectronic devices. Therefore, it is still a challenge to explore computationally and structurally the semiconductivity of COFs and to determine their final potential. Herein, we report on the possible semiconducting properties and results of polyimide–COF materials using density functional theory calculations. Our analysis includes monolayers and multilayers (AA- and AB-stacked modes) of mellitic triimide frameworks designed from mellitic trianhydride (MTA) as the main building knot, including MTI-TAPB-COF, which was previously synthesized from the condensation reaction of MTA and 1,3,5-tris(4-aminophenyl)benzene (TAPB), and other previously unreported structures based on MTA. Respective frameworks have been selected due to the difference in building block symmetry ($C_3 + C_2$ and $C_3 + C_3$) and different chemical linkages, either by benzene or by pyridine rings. We find the polyimide multilayers to be stable and with varying electronic properties. The finite band gap exhibited by every structure (monolayer and stacked) was sensitive to atomic arrangement. Stacking introduces dispersion to an otherwise flat band structure of the materials, which appeared to be highly sensitive to stacking direction. The effect of stacking was similar for each COF, but the magnitude of band structure change was different and dependent on the symmetry of the building blocks.



INTRODUCTION

Polyimide-linked covalent organic frameworks (COFs) represent a relatively unexplored class of two-dimensional (2D) semiconducting polymers in spite of their unique electronic properties.¹ Polyimide semiconductors are generally constructed structurally by alternating imide ring (acceptor) and (amine) phenyl (donor) residues,² whose interactions determine their electronic properties. A distinctive feature is the existence of intramolecular charge transfer between the segments.³ The structure of the polymer plays an important role in determining the charge-transfer properties in terms of its primary^{4,5} and secondary-order⁶ conformations.

In the case of 2D COFs, the primary structure (in-plane bonding) is determined by covalent bonds formed in the polycondensation reaction of building blocks, while the secondary structure (out-of-plane bonding) is the result of van der Waals forces, leading to the creation of stacked layers in the out-of-plane direction.⁷ This means that the electronic properties of the COF can be tuned by engineering the linkages or by controlling the π – π stacking between each COF

layer.⁸ The latter approach has been demonstrated computationally for sp^2 -carbon-conjugated COFs, showing a high sensitivity of the electronic band-gap width and band dispersion on the stacking direction.⁹ Here, we investigate similar effects in COFs that contain carbon and a significant percentage of nitrogen atoms and not just sp^2 -hybridized carbon. Both of these factors disorganize the π – π stacking interaction by themselves. This work introduces another factor that has not been studied yet: a different rotational symmetry of building blocks of the polyimide COFs.

The MTI-TAPB-COF (reported previously under the name MTI-COF-1) with mellitic triimide knots and phenylene

Received: August 30, 2023
Revised: November 15, 2023
Accepted: November 16, 2023
Published: December 5, 2023



linkers in a $[C_3 + C_3]$ topology was previously analyzed before with energy storage and gas separation applications in mind.¹⁰ In that work, one of the COFs was created by linking MTA and TAPB in a polycondensation reaction. It had been synthesized and characterized in terms of its structure, porosity, and sorption capability. However, the electronic properties of the compound were not been analyzed. Herein, we examined and compared the MTI-TAPB-COF material to a few not-yet-synthesized compounds with $[C_3 + C_3]$ and $[C_3 + C_2]$ topologies. We focused on key differences in the structure. One focus is the different rotational symmetry of the building blocks and their effect on the band structure. To add another dimension to our analysis, for each building block symmetry configuration, we considered two types of structures. One $[C_3 + C_3]$ COF was linked with a C_3 linker that contained benzene rings (1,3,5-tris(4-aminophenyl) benzene, TAPB), while the other C_3 linker was built using pyridine rings (1,3,5-tris(4-aminopyridyl) pyridine, TAPyrPyr). Similarly, in $[C_3 + C_2]$ COFs, a benzene-based linker (*p*-phenylenediamine, PPD) and a pyridine-based linker (2,5-diaminopyridine, DAPyr) were used. In total, four COF structures were analyzed, as depicted in Figure 1. Therefore, in addition to the rotational symmetry,

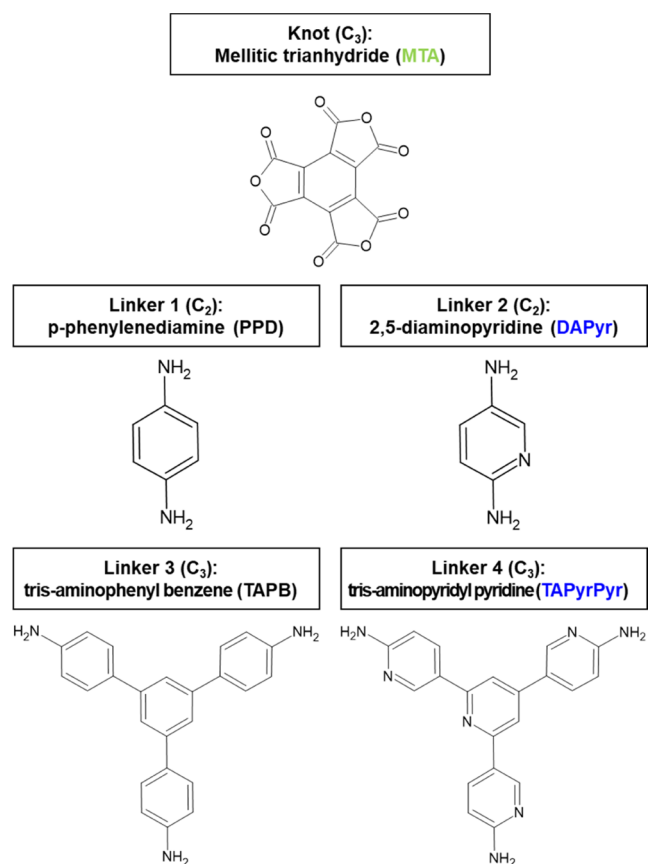


Figure 1. Building blocks and structure of MTI-DAPyr-COF and MTI-TAPB-COF.

we also changed the chemical structure of the linker unit by introducing pyridine rings in place of benzene. The introduction of a pyridine ring, i.e., the replacement of the carbon atom of the benzene ring with a highly electronegative nitrogen atom, is expected to alter the electronic band gap of the framework.¹¹ This change allowed us to analyze the change of the donor–donor character of the experimentally synthe-

sized MTI-TAPB-COF to the donor–acceptor structure of the new COFs. The use of electron donor–acceptor COFs presents new opportunities for applications in semiconductor devices⁸ and has already been demonstrated to have desirable optoelectronic properties.^{12–14}

RESULTS AND DISCUSSION

The structure of the MTI-(PPD/DAPyr)-COF (depicted schematically in Figure 2) is typical for a C_3 – C_2 COF and consists of two knots and three linker units. On the other hand, the C_3 – C_3 compound MTI-(TAPB/TAPyrPyr)-COF consists of one knot and one linker unit. When discussing thermodynamic stability, the difference in total energies will be expressed per unit cell relative to the relaxed monolayer configuration. This leads to the expression for the stacking energy, $E_{\text{stacking}} = E_{\text{AA/AB}} - 2^*E_{\text{monolayer}}$. In addition to the total energy stability metric, we analyzed the density functional theory (DFT)-optimized interlayer distance expressed by out-of-plane unit cell vector length c and the dispersion energy, which determines the strength of the van der Waals interaction. All of these quantities, along with the parameters related to the electronic band structures, are listed for each analyzed structure in Table 1.

In terms of stacking energy, all of the stacked configurations for all COFs are preferred over the free-standing monolayers on the order of a few dozen kcal mol⁻¹. The benzene-containing structures MTI-PPD and MTI-TAPB stack preferentially in the AA mode. The difference in total energies between AA and AB configurations is -9.59 kcal mol⁻¹ in the case of the PPD linker and -14.02 kcal mol⁻¹ for the TAPB linker. On the other hand, the energy of COFs linked by pyridine rings, MTI-DAPyr and MTI-TAPyrPyr, is the lowest for AB stacking. However, the difference between the most preferred stackings is lower at 0.68 kcal mol⁻¹ (DAPyr) and 3.26 kcal mol⁻¹ (TAPyrPyr). Thermodynamics of stacking therefore appear to be determined more so by the chemical composition than by symmetry of the building blocks.

The dispersion energy, calculated by the D3 method (Methods Section), is similar for each monolayer cell. The lower values (by the order of two) found for stacked structures are attributed to the van der Waals interaction between neighboring stacked pores. By comparing the dispersion energy between different structures and to the stacking energy of the same structure, we could identify the DFT-D3 dispersion component as the key interaction contributing to the stability of the structures. For instance, the MTI-PPD-AA configuration exhibited a dispersion energy lower by 14 kcal mol⁻¹ than the AB configuration. The dispersion interaction also stabilizes the structure of the AA mode of MTI-DAPyr, the second C_3 – C_2 structure in the analysis, by 18 kcal mol⁻¹. For the C_3 – C_3 structures, the AB mode dispersion interaction stabilizes the structures more by a smaller margin of 5 kcal mol⁻¹ for MTI-TAPB and 7 kcal mol⁻¹ for MTI-TAPyrPyr. This difference between C_3 – C_2 and C_3 – C_3 topologies is due to the fact that the C_3 – C_2 symmetry leads to a more commensurate arrangement of aromatic rings between subsequent layers of COF, which increases the amount of the π – π interaction in the system (Figure 3).

The valence and conduction bands of each monolayer COF can be very well approximated by fully flat bands in every direction of the reciprocal lattice. The monolayer band gap is between 2.16 eV (MTI-TAPB) and 2.72 eV (MTI-DAPyr).

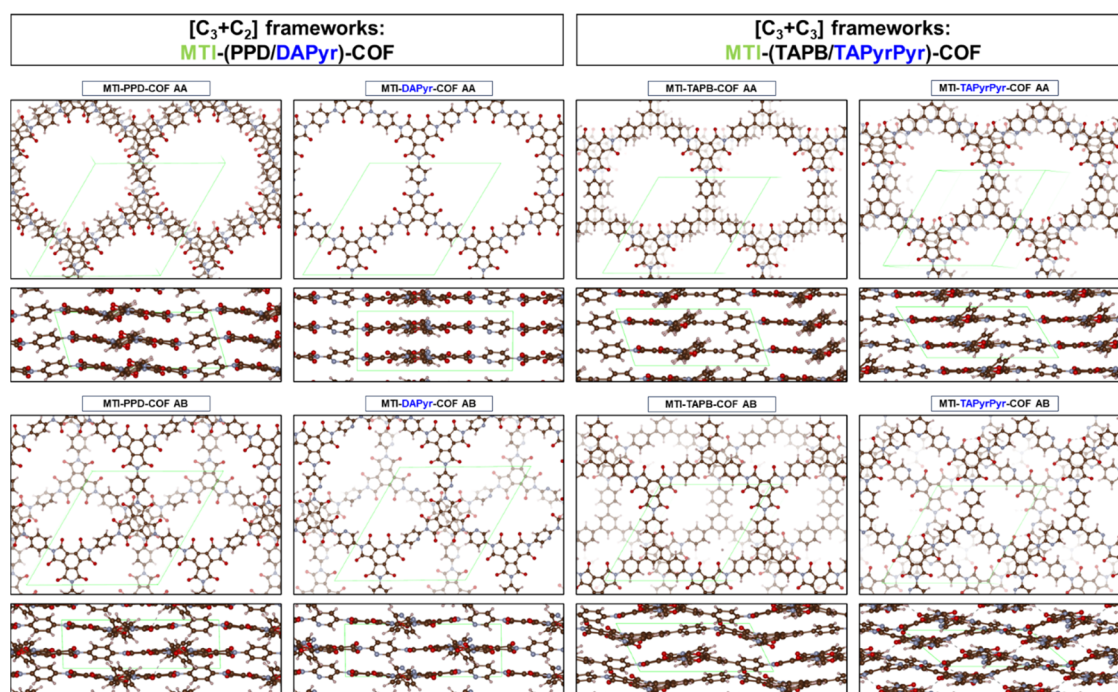


Figure 2. Top and side views depict the relaxed geometries of each structure and stacking mode.

Table 1. DFT Calculation Results of Stacked Polyimide COFs: Out-of-Plane Unit Cell Vector Length (c), Dispersion and Stacking Energies, and Amount of Valence Band (VB) and Conduction Band (CB) Dispersions between Γ and Z High-Symmetry Points in the First Brillouin Zone

COF	stacking mode	c (Å)	D3 dispersion energy per unit cell (kcal mol ⁻¹)	stacking energy per unit cell (kcal mol ⁻¹)	band gap (eV)	$\Gamma \rightarrow Z$ VB dispersion (eV)	$\Gamma \rightarrow Z$ CB dispersion (eV)
MTI-PPD (C ₃ -C ₂ , benzene)	monolayer		-42		2.35		
	AA (relaxed)	3.45	-95	-68.62	1.10	-0.81	0.40
	AB (relaxed)	2.92	-81	-59.03	1.67	-0.15	-0.24
	monolayer		-40		2.72		
MTI-DAPyr (C ₃ -C ₂ , pyridine)	AA (relaxed)	3.48	-90	-59.09	1.29	-0.56	0.45
	AB (relaxed)	3.16	-72	-59.77	2.08	-0.03	-0.11
MTI-TAPB (C ₃ -C ₃ , benzene)	monolayer		-34		2.16		
	AA (relaxed)	3.56	-79	-72.21	1.19	-0.42	0.21
	AB (relaxed)	3.29	-84	-58.19	1.85	0.02	-0.03
	monolayer		-32		2.53		
MTI-TAPyrPyr (C ₃ -C ₃ , pyridine)	AA (relaxed)	3.59	-78	-45.02	1.20	-0.39	0.49
	AB (relaxed)	3.49	-85	-48.28	1.85	0.09	0.08

Band gaps for benzene-linked COFs are noticeably lower than those for pyridine-linked ones.

When stacked in the AA mode, the differences between different COFs are diminished, and their band gaps are all between 1.10 and 1.29 eV. The closing of the band gap is accompanied by a significant dispersion in the reciprocal lattice directions in which the out-of-plane component (along the c axis) changes. These are the Γ -Z, Γ -N, Γ -M, and Γ -R directions. In the remaining directions Γ -X, Γ -Y, and Γ -L, in which the out-of-plane component does not change, the bands that define the electronic gap remain flat. The amount of band dispersion is quantified by the change in energy of the frontier

bands between the Γ and Z points. Dispersion is particularly pronounced in the AA mode of all COFs for both holes and electrons. Dispersion of conduction band electrons is the smallest for MTI-TAPB (0.21 eV), while for the rest of the structures, it is on the order of 0.4–0.5 eV. The $\Gamma \rightarrow Z$ dispersion is, in each AA structure, negative for holes and positive for electrons, meaning that the Γ point is both the valence band maximum (VBM) and conduction band minimum (CBM). The resulting band gap is thus direct.

In the AB mode, the band gaps show intermediate values between those of the monolayers and AA structures. There is a noticeable dispersion of the frontier bands, however, in a

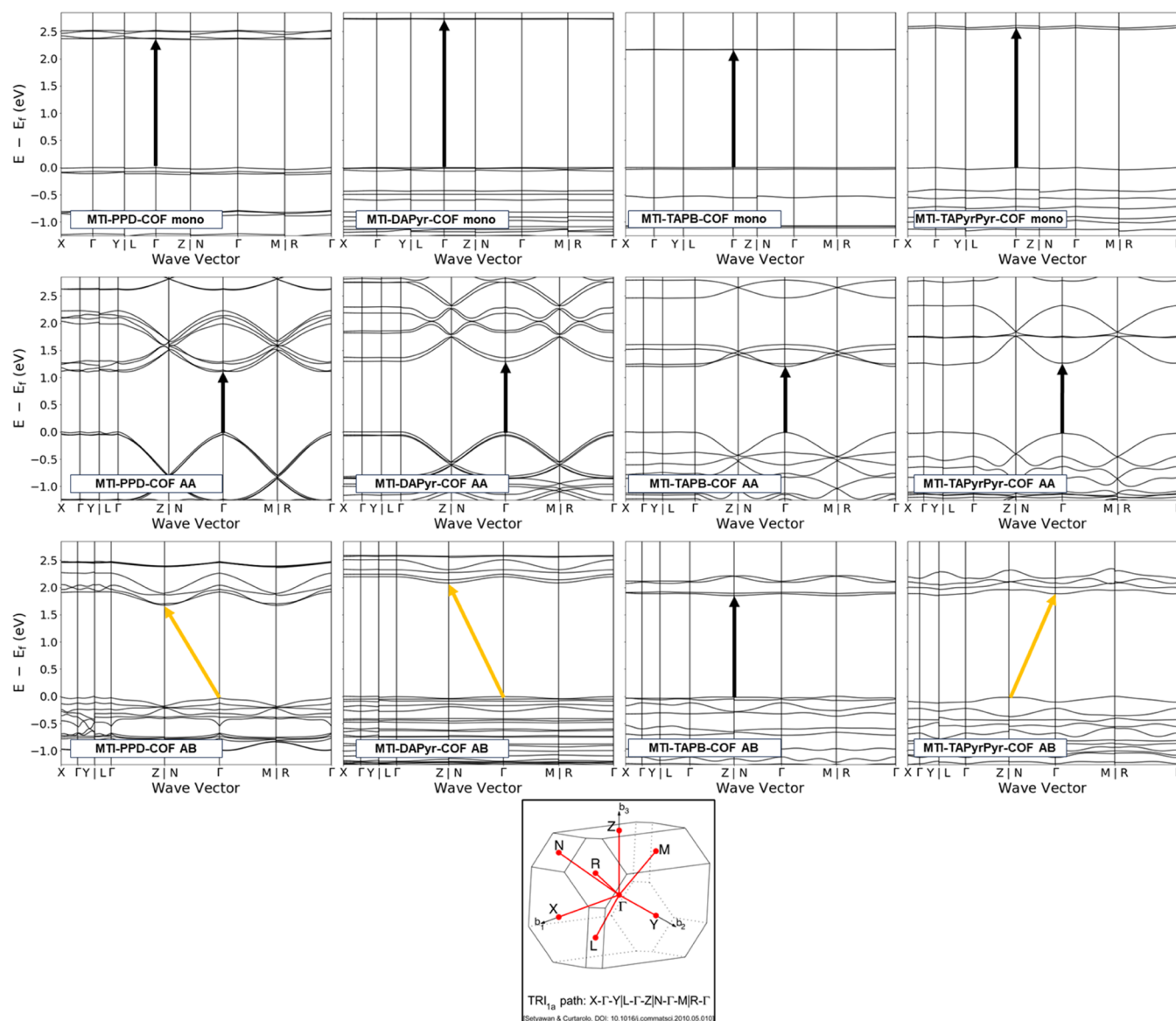


Figure 3. Band structure of monolayer, AA, and AB configurations of all calculated COF structures. The black and yellow arrows denote direct and indirect transitions, respectively.

smaller order than in the case of the AA structure. Notably, the sign of the dispersion relation is no longer negative for VB and positive for CB depending on the AB structure. This means that the Γ -point band energy does not necessarily define the band-gap transition. In the case of MTI-PPD and MTI-DAPyr, the lowest energy band transition is Γ -Z; in MTI-TAPyrPyr, it is Z- Γ . Because of the smaller band curvature between these points, the band gaps are only weakly indirect in these cases. The most narrow and indirect band gap was calculated for MTI-PPD.

CONCLUSIONS

Following the previously described successful synthesis of polyimide covalent organic frameworks with building blocks exhibiting the $[C_3 + C_3]$ symmetry, we calculated and closely followed their theoretical electronic properties and compared them to three chemically and structurally similar but not-yet-synthesized frameworks. The comparison was based on three factors: (I) building block symmetry by comparing to COFs

with the $[C_3 + C_2]$ topology, (II) chemical structure of the linker unit by linking either via benzene rings or pyridine rings, and (III) the stacking modes of COFs, either AA or AB. As we found out, the building block symmetry influenced the dispersion energy in the form of π - π stacking. This effect was most pronounced in AA COFs. Linking the COF via pyridine linkers introduced a higher band gap compared to benzene linkers. While the thermodynamic quantities for different stacked structures varied between different COFs, the band gaps and band dispersions were similar across structures with the same stacking mode. The free-standing monolayer COFs all featured completely flat band structures. Stacked structures introduced lighter electrons and holes, particularly in the case of the AA stacking mode. More stable AA structures and a higher energetic separation between AA and AB stacking modes present in benzene-linked COFs may prove to be advantageous in terms of their selective synthesis. This will likely prove to be important for successful applications in optoelectronic devices. On the other hand, the pyridine-linked



Figure 4. General workflow of methods and computational tools used in this study. See the text for more detailed information about the methodology.

COFs show the most dispersion in the conduction and offer the lightest conduction electrons in the AA configuration.

Stacking the COFs shifts the band gap from the lower ultraviolet range to the lower end of the visible range, making the structures' properties more interesting for optoelectronic applications. In particular, the increased photon absorption in the part of the solar spectrum usable for photovoltaic conversion close to the Shockley–Queisser limit could make such structures desirable for solar-cell applications. As a whole, better control of stacking directions during the growth of the materials, translating into tunable band gaps and other electronic properties, should allow new semiconductor devices based on polyimide 2D COFs to emerge.

METHODS

Geometry optimizations have been performed by the plane-wave DFT method implemented in the VASP^{15–18} package, with PAW¹⁹ pseudopotentials expressed in the plane-wave basis set with a cutoff of 400 eV. The DFT-D3(BJ) dispersion correction^{20,21} was used to account for van der Waals forces. For the geometry optimization calculations, the PBEsol functional²² was used and only the Γ k-point was used to calculate ionic forces. Optimization of the ionic positions was performed until forces acting on ions vanished below 0.05 eV/Å. The monolayer system was optimized in two steps. Initially, the general AMBER force field (GAFF)^{23,24} relaxation was applied in order to find the approximate relaxed geometry. Afterward, DFT optimization was performed. The unit cell was fixed at 20 Å in the z direction. This allowed us to consider only the in-plane interactions present in the primary structure of the COF. Then, the AA-stacked structure was created by creating a $1 \times 1 \times 2$ supercell of the monolayer structure and re-minimizing the ionic forces. All atomic and cell degrees of freedom were allowed to change during the relaxation. Next, the AB-stacked structure was created by shifting the atomic positions of one of the AA-stacked layers by an $(a/3, -2b/3, 0)$ vector, expressed in fractional AA unit cell parameters. Then, another reoptimization of atomic positions and unit cell vectors was performed for the AB structure (Figure 4).

The three optimized structures—monolayer, AA-stacked, and AB-stacked—were used in band structure calculations. The HSE06²⁵ hybrid functional was used to calculate band energies. After initial convergence on a $4 \times 4 \times 4$ k-point grid, the same grid with additional k-points along the high-symmetry path was converged until a 10^{-7} eV threshold was reached. Since all of the structures were in the space group P1 triclinic symmetry, the standard k-point path $X \rightarrow \Gamma \rightarrow Y | L \rightarrow \Gamma \rightarrow Z | N \rightarrow \Gamma \rightarrow M | R \rightarrow \Gamma$ was used, denoted TR1_{1a} by Setyawan & Curtarolo.²⁶ Preparation of calculation and data analysis was performed using Python scripts with the use of the Pymatgen library,²⁷ and structures were visualized with VESTA.²⁸

ASSOCIATED CONTENT

Supporting Information

The Supporting Information is available free of charge at <https://pubs.acs.org/doi/10.1021/acsomega.3c06496>.

- DFT-optimized crystal structure of MTI-PPD, monolayer configuration (CIF)
- DFT-optimized crystal structure of MTI-PPD, AA stacking mode (CIF)
- DFT-optimized crystal structure of MTI-PPD, AB stacking mode (CIF)
- DFT-optimized crystal structure of MTI-DAPyr, monolayer configuration (CIF)
- DFT-optimized crystal structure of MTI-DAPyr, AA stacking mode (CIF)
- DFT-optimized crystal structure of MTI-DAPyr, AB stacking mode (CIF)
- DFT-optimized crystal structure of MTI-TAPB, monolayer configuration (CIF)
- DFT-optimized crystal structure of MTI-TAPB, AA stacking mode (CIF)
- DFT-optimized crystal structure of MTI-TAPB, AB stacking mode (CIF)
- DFT-optimized crystal structure of MTI-TAPyrPyr, monolayer configuration (CIF)
- DFT-optimized crystal structure of MTI-TAPyrPyr, AA stacking mode (CIF)
- DFT-optimized crystal structure of MTI-TAPyrPyr, AB stacking mode (CIF)

AUTHOR INFORMATION

Corresponding Authors

Mateusz Wlazlo – Next-Generation Energy Systems Group, Centre of Excellence ENSEMBLE3, Warsaw 01-919, Poland; Present Address: Chemical and Biological Systems Simulation Lab, Centre of New Technologies, University of Warsaw, 02-097 Warsaw, Poland; Current E-mail: m.wlazlo@cent.uw.edu.pl; orcid.org/0000-0001-5493-3154; Email: mateusz.wlazlo@ensemble3.eu

Atsushi Nagai – Next-Generation Energy Systems Group, Centre of Excellence ENSEMBLE3, Warsaw 01-919, Poland; orcid.org/0000-0002-5871-1775; Email: atsushi.nagai@ensemble3.eu

Author

Keiichiro Maegawa – Next-Generation Energy Systems Group, Centre of Excellence ENSEMBLE3, Warsaw 01-919, Poland; Department of Electrical and Electronic Information Engineering, Toyohashi University of Technology, Toyohashi, Aichi 441-8580, Japan

Complete contact information is available at: <https://pubs.acs.org/10.1021/acsomega.3c06496>

Notes

The authors declare no competing financial interest.

ACKNOWLEDGMENTS

The authors thank the “ENSEMBLE3—Centre of Excellence for nanophotonics, advanced materials and novel crystal growth-based technologies” project (GA No. MAB/2020/14) carried out within the International Research Agendas programme of the Foundation for Polish Science cofinanced by the European Union under the European Regional Development Fund and the European Union’s Horizon 2020 research and innovation programme teaming for Excellence (GA. No. 857543) for support of this work. The authors gratefully acknowledge Poland’s high-performance computing infrastructure PLGrid (HPC Centers: ACK Cyfronet AGH) for providing computer facilities and support within computational grant no. PLG/2022/015965 and PLGrid for awarding this project access to the LUMI supercomputer, owned by the EuroHPC Joint Undertaking, hosted by CSC (Finland) and the LUMI consortium through grant no. PLL/2022/03/016435.

REFERENCES

- (1) Salley, J. M.; Frank, C. W. Charge Transfer in Aromatic Polyimides. In *Polyimides*; Ghosh, M.; Mittal, K. L., Eds.; CRC Press: Boca Raton, 2018; pp 279–307.
- (2) Kotov, B. V.; Gordina, T.; Voishchev, V.; et al. Aromatic polyimides as charge transfer complexes. *Polym. Sci. U.S.S.R.* **1977**, *19* (3), 711–716.
- (3) Salley, J. M.; Miwa, T.; Frank, C. W. Intramolecular Charge Transfer In Aromatic Polyimides. *MRS Proc. Libr.* **1991**, *227*, 117–124, DOI: 10.1557/PROC-227-117.
- (4) LaFemina, J. P.; Arjavalingam, G.; Hougham, G. Electronic structure and ultraviolet absorption spectrum of polyimide. *J. Chem. Phys.* **1989**, *90* (9), 5154–5160.
- (5) Wachsmann, E. D.; Frank, C. W. Effect of cure history on the morphology of polyimide: Fluorescence spectroscopy as a method for determining the degree of cure. *Polymer* **1988**, *29* (7), 1191–1197.
- (6) Kazaryan, L. G.; Tsvankin, D.; Ginzburg, B.; et al. X-ray diffraction study of the crystalline structure of aromatic polyimides. *Polym. Sci. U.S.S.R.* **1972**, *14* (5), 1344–1354.
- (7) Tan, K. T.; Ghosh, S.; Wang, Z.; et al. Covalent organic frameworks. *Nat. Rev. Methods Primers* **2023**, *3*, No. 1, DOI: 10.1038/s43586-022-00181-z.
- (8) Keller, N.; Bein, T. Optoelectronic processes in covalent organic frameworks. *Chem. Soc. Rev.* **2021**, *50* (3), 1813–1845.
- (9) Kuc, A.; Springer, M. A.; Batra, K.; et al. Proximity Effect in Crystalline Framework Materials: Stacking-Induced Functionality in MOFs and COFs. *Adv. Funct. Mater.* **2020**, *30* (41), No. 1908004, DOI: 10.1002/adfm.201908004.
- (10) Veldhuizen, H.; Vasileiadis, A.; Wagemaker, M.; et al. Synthesis, characterization, and CO₂ uptake of mellitic triimide-based covalent organic frameworks. *J. Polym. Sci., Part A: Polym. Chem.* **2019**, *57* (24), 2373–2377.
- (11) Hooge, F. N. Relation between Electronegativity and Energy Bandgap. *Z. Phys. Chem.* **1960**, *24* (3_4), 275–282, DOI: 10.1524/zpch.1960.24.3_4.275.
- (12) Guo, J.; Xu, Y.; Jin, S.; et al. Conjugated organic framework with three-dimensionally ordered stable structure and delocalized pi clouds. *Nat. Commun.* **2013**, *4*, No. 2736, DOI: 10.1038/ncomms3736.
- (13) Calik, M.; Auras, F.; Salonen, L. M.; et al. Extraction of photogenerated electrons and holes from a covalent organic framework integrated heterojunction. *J. Am. Chem. Soc.* **2014**, *136* (51), 17802–17807.
- (14) Jin, S.; Supur, M.; Addicoat, M.; et al. Creation of Superheterojunction Polymers via Direct Polycondensation: Segre-

gated and Bicontinuous Donor-Acceptor pi-Columnar Arrays in Covalent Organic Frameworks for Long-Lived Charge Separation. *J. Am. Chem. Soc.* **2015**, *137* (24), 7817–7827, DOI: 10.1021/jacs.5b03553.

(15) Kresse, G.; Hafner, J. Ab initio molecular dynamics for liquid metals. *Phys. Rev. B* **1993**, *47* (1), 558–561.

(16) Kresse, G.; Hafner, J. Ab initio molecular-dynamics simulation of the liquid-metal-amorphous-semiconductor transition in germanium. *Phys. Rev. B* **1994**, *49* (20), 14251–14269.

(17) Kresse, G.; Furthmüller, J. Efficiency of ab-initio total energy calculations for metals and semiconductors using a plane-wave basis set. *Comput. Mater. Sci.* **1996**, *6* (1), 15–50.

(18) Kresse, G.; Furthmüller, J. Efficient iterative schemes for ab initio total-energy calculations using a plane-wave basis set. *Phys. Rev. B* **1996**, *54* (16), 11169–11186.

(19) Kresse, G.; Joubert, D. From ultrasoft pseudopotentials to the projector augmented-wave method. *Phys. Rev. B* **1999**, *59* (3), 1758–1775.

(20) Grimme, S.; Antony, J.; Ehrlich, S.; et al. A consistent and accurate ab initio parametrization of density functional dispersion correction (DFT-D) for the 94 elements H-Pu. *J. Chem. Phys.* **2010**, *132* (15), No. 154104.

(21) Grimme, S.; Ehrlich, S.; Goerigk, L. Effect of the damping function in dispersion corrected density functional theory. *J. Comput. Chem.* **2011**, *32* (7), 1456–1465.

(22) Perdew, J. P.; Ruzsinszky, A.; Csonka, G. I.; et al. Restoring the density-gradient expansion for exchange in solids and surfaces. *Phys. Rev. Lett.* **2008**, *100* (13), No. 136406.

(23) Wang, J.; Wolf, R. M.; Caldwell, J. W.; et al. Development and testing of a general amber force field. *J. Comput. Chem.* **2004**, *25* (9), 1157–1174.

(24) Wang, J.; Wang, W.; Kollman, P. A.; et al. Automatic atom type and bond type perception in molecular mechanical calculations. *J. Mol. Graphics Modell.* **2006**, *25* (2), 247–260.

(25) Krukau, A. V.; Vydrov, O. A.; Izmaylov, A. F.; et al. Influence of the exchange screening parameter on the performance of screened hybrid functionals. *J. Chem. Phys.* **2006**, *125* (22), No. 224106.

(26) Setyawan, W.; Curtarolo, S. High-throughput electronic band structure calculations: Challenges and tools. *Comput. Mater. Sci.* **2010**, *49* (2), 299–312.

(27) Ong, S. P.; Richards, W. D.; Jain, A.; et al. Python Materials Genomics (pymatgen): A robust, open-source python library for materials analysis. *Comput. Mater. Sci.* **2013**, *68*, 314–319.

(28) Momma, K.; Izumi, F. VESTA 3 for three-dimensional visualization of crystal, volumetric and morphology data. *J. Appl. Crystallogr.* **2011**, *44* (6), 1272–1276.